# Solution Structures of Apo and Holo Biotinyl Domains from Acetyl Coenzyme A Carboxylase of *Escherichia coli* Determined by Triple-Resonance Nuclear Magnetic Resonance Spectroscopy†

Emma L. Roberts,‡,§ Ningcheng Shu,‡,§ Mark J. Howard,‡ R. William Broadhurst,‡ Anne Chapman-Smith,|| John C. Wallace,|| Tim Morris,⊥ John E. Cronan, Jr.,⊥ and Richard N. Perham*,‡

*Cambridge Centre for Molecular Recognition, Department of Biochemistry, University of Cambridge, 80 Tennis Court Road, Cambridge CB2 1GA, U.K., Department of Biochemistry, University of Adelaide, Adelaide, South Australia 5005, Australia, and Department of Microbiology, University of Illinois, B103 Chemical and Life Sciences Laboratory, 601 South Goodwin Avenue, Urbana, Illinois 61801*

*Received October 15, 1998; Revised Manuscript Received February 3, 1999*

ABSTRACT: A subgene encoding the 87 C-terminal amino acids of the biotinyl carboxy carrier protein (BCCP) from the acetyl CoA carboxylase of *Escherichia coli* was overexpressed and the apoprotein biotinylated in vitro. The structures of both the apo and holo forms of the biotinyl domain were determined by means of multidimensional NMR spectroscopy. That of the holo domain was well-defined, except for the 10 N-terminal residues, which form part of the flexible linker between the biotinyl and subunit-binding domains of BCCP. In agreement with X-ray crystallographic studies [Athappilly, F. K., and Hendrickson, W. A. (1995) *Structure 3*, 1407−1419], the structure comprises a flattened $\beta$-barrel composed of two four-stranded $\beta$-sheets with a 2-fold axis of quasi-symmetry and the biotinyl-lysine residue displayed in an exposed $\beta$-turn on the side of the protein opposite from the N- and C-terminal residues. The biotin group is immobilized on the protein surface, with the ureido ring held down by interactions with a protruding polypeptide "thumb" formed by residues 94−101. However, at the site of carboxylation, no evidence could be found in solution for the predicted hydrogen bond between the main chain O of Thr94 and the ureido $H^{N1'}$. The structure of the apo domain is essentially identical, although the packing of side chains is more favorable in the holo domain, and this may be reflected in differences in the dynamics of the two forms. The thumb region appears to be lacking in almost all other biotinyl domain sequences, and it may be that the immobilization of the biotinyl-lysine residue in the biotinyl domain of BCCP is an unusual requirement, needed for the catalytic reaction of acetyl CoA carboxylase.

Acetyl coenzyme A carboxylase (ACC)[1] (EC 6.4.1.2) catalyzes the initial committed step in the de novo biosynthesis of long-chain fatty acids through the carboxylation of acetyl CoA to form malonyl CoA. The ACC enzyme complex from *Escherichia coli* can readily be resolved into its three functional components: biotin carboxylase (BC), a homodimer of protein subunits each with a molecular mass of 49 kDa (*1*); the biotin carboxy carrier protein (BCCP), a homodimer (*2*) of polypeptide chains each of which contains 156 amino acids, as deduced from the DNA sequence of the corresponding gene (*3*); and carboxyl transferase (CT), an $\alpha_2\beta_2$ heterotetramer of $\alpha$- and $\beta$-subunits with molecular masses of 35 and 30 kDa, respectively (*1*, *4*). The functional enzyme contains two copies of each of the four proteins, but readily falls apart into CT and a BCCP−BC subcomplex.

BCCP has two roles, structural and mechanistic, in ACC. It acts to bind the BC component, thereby bringing it into physical proximity for the catalysis of the carboxylation reaction, and it serves as a carboxyl group carrier in the overall enzymic mechanism. A biotinyl group is attached post-translationally to BCCP by a biotinyl protein ligase (BPL, also known as biotin holoenzyme synthetase), which catalyzes the formation of an amide linkage between the carboxy group of the biotin and the $N^6$-amino group of a specific lysine residue. Thus, the functional bicyclic ring of biotin is attached via a potentially flexible 1.4 nm side chain to the polypeptide backbone of BCCP, and is therefore capable in principle of linking active sites up to 2.8 nm apart. In the first reaction, BC utilizes $CO_2$ to carboxylate the biotin ring, the N1′ ureido proton being replaced by a carboxyl

† This work was supported by research grants from the Biotechnology and Biological Sciences Research Council (to R.N.P.), the Australian Research Council (AO9531996 to J.C.W.), and the National Institutes of Health (AI15650 to J.E.C.). The core facilities of the Cambridge Centre for Molecular Recognition are supported by the BBSRC and The Wellcome Trust. E.L.R. was a recipient of a Research Studentship from the Medical Research Council, and N.S. was supported by a Research Studentship from the Oppenheimer Fund, University of Cambridge, and a bursary from the Cambridge Overseas Trust.

* To whom correspondence should be addressed. Telephone: (+44) (0)1223 333663. Fax: (+44) (0)1223 766002. E-mail: r.n.perham@bioc.cam.ac.uk.

‡ University of Cambridge.

§ These authors contributed equally to this work.

|| University of Adelaide.

⊥ University of Illinois.

[1] Abbreviations: DQF-COSY, double-quantum filtered correlation spectroscopy; HMQC, heteronuclear multiple-quantum coherence; HSQC, heteronuclear single-quantum coherence; NOE, nuclear Overhauser effect; NOESY, nuclear Overhauser enhancement spectroscopy; PAGE, polyacrylamide gel electrophoresis; TOCSY, total correlation spectroscopy.

10.1021/bi982466o CCC: $18.00 
Published on Web 04/02/1999

group (*5*). The carboxylated biotin then moves to the active site of CT, where the carboxyl group is transferred to acetyl CoA, to yield the product malonyl CoA. The biotinyl-lysine residue is located in the C-terminal region of the BCCP polypeptide chain, in an independently folded domain of about 80 amino acids which can be isolated in apo and holo forms (*6*−*8*).

In many ways, therefore, the biotinyl domains of ACC and other biotin-dependent carboxylases (*5*, *9*) resemble the lipoyl domains of 2-oxo acid dehydrogenase multienzyme complexes, in which a lipoyllysine residue helps to ferry substrate between the three active sites represented in these multifunctional proteins (*10*−*12*). Structures of the 80-residue lipoyl domains from various 2-oxo acid dehydrogenase complexes have been determined by means of NMR spectroscopy (*13*−*17*) and found to consist of two four-stranded $\beta$-sheets with a 2-fold axis of quasi-symmetry. The lipoyllysine residue is prominently displayed in a tight $\beta$-turn in the $\beta$-sheet opposite that containing the N- and C-terminal residues of the domain, and there is no evidence of a major conformational change accompanying post-translational attachment of the lipoyl group, which is essentially free to rotate on the surface of the protein.

Despite minimal amino acid sequence similarity (*18*), the structure of the biotinyl domain was predicted to resemble that of the lipoyl domain (*19*) and the determination of the structure of the biotinylated domain from *E. coli* ACC (residues 77−156 of BCCP) by means of X-ray crystallography has borne out that prediction (*20*). Again, the structure is that of a flattened $\beta$-barrel comprising two four-stranded $\beta$-sheets with a 2-fold axis of quasi-symmetry, and the biotinyl-lysine residue displayed in a $\beta$-turn on the side of the protein opposite from the N- and C-terminal residues. However, there is one striking and unexpected feature of the structure. The biotin group is localized on the protein surface, with the ureido ring rendered somewhat inaccessible and held down by interactions with a protruding protein "thumb" formed by residues 94−101 (*20*). These interactions are highly specific, not the least being a hydrogen bond between the main chain O of Thr94 and the ureido $H^{N1'}$.

A structure of the apo form of the biotinyl domain *E. coli* ACC has been determined by means of NMR spectroscopy (*21*), and some slight differences between the holo and apo forms of the domain were reported. However, the comparison was drawn with the structure of the domain as determined by X-ray crystallography (*20*), and a direct comparison of the holo and apo forms based on the same structural technique remained to be made. Moreover, the localization of the biotinyl-lysine swinging arm on the surface of the domain, as indicated in the X-ray structure, has implications for the catalytic mechanism; it is essential to demonstrate that it is not an artifact of the crystallization procedure. Indeed, it has recently been reported that there is no interaction between the biotinyl group and the protein in the 1.3S subunit of the enzyme transcarboxylase from *Propionibacterium shermanii* (*22*). In this paper, we describe the determination of the solution structures of both the holo and apo forms of the biotinyl domain of *E. coli* ACC by means of triple-resonance NMR spectroscopy and an investigation of the existence and strength of the hydrogen bond thought to involve the ureido $H^{N1'}$, the site of carboxylation of the biotin ring.

## MATERIALS AND METHODS

*Preparation of the Apo and Holo Forms of the Biotinyl Domain*. Uniformly $^{13}C$- and $^{15}N$-labeled and $^{15}N$-labeled samples were prepared by expressing the biotin domain subgene from plasmid pTM53 (*7*) in *E. coli* strain BL21$\lambda$DE3 in morpholinepropanesulfonate (MOPS) minimal medium (*23*). The medium contained either 0.14% [$^{13}C$]glucose and 9.5 mM $^{15}NH_4Cl$ as the sole carbon or nitrogen source for the doubly labeled proteins or 0.35% glucose and 9.5 mM $^{15}NH_4Cl$ for the singly labeled proteins. Preliminary experiments showed that at these concentrations, the limiting isotopically labeled nutrients were exhausted 3 h after induction of protein expression, thus ensuring maximal incorporation of label. Expression of the domain in a strain in which biotin protein ligase is expressed from the coresident plasmid pCY216 results in partial biotinylation in vivo (*7*). Therefore, to avoid producing protein with a mixture of isotopes in the biotinyl moiety, the fermentations for isotopic labeling were carried out in strains carrying only the chromosomal copy of the biotin ligase gene. This resulted in the production of greater than 99% of the domain in the apo form (data not shown). To produce the holo domains, biotinylation was performed in vitro in crude cell lysates, prepared as described by Chapman-Smith et al. (*7*), by addition of 3 mM ATP, 0.4 mM biotin, and a lysate from cells expressing biotin protein ligase from pCY216 (*7*). Unlabeled samples of apo and holo domains from *E. coli* ACC were prepared, and all proteins were purified according to the method of Chapman-Smith et al. (*7*). Where necessary, additional purification was carried out using a Superdex75 (Pharmacia) gel filtration column (2.6 cm × 60 cm) with a flow rate of 2 mL/min in 50 mM sodium MOPS (pH 7.2), 0.15 M NaCl, 0.1 mM EDTA, and 0.2 mM dithiothreitol.

*NMR Spectroscopy*. For NMR spectroscopy, protein samples with a concentration of approximately 3 mM were made up in 20 mM sodium phosphate buffer (pH 6.8) and 90% $^1H_2O$/10% $^2H_2O$. The following experiments were performed at 303 K as described either by Kraulis et al. (*24*) or in the original references. The two-dimensional (2D) DQF-COSY, NOESY, [$^{15}N$,$^1H$]-HSQC, HNHB, *J*-modulated [$^{15}N$,$^1H$]-COSY, and {$^1H$}−$^{15}N$ heteronuclear NOE spectra were acquired using a Bruker AM500 spectrometer. Spectra from the three-dimensional (3D) $^{15}N$-separated NOESY-HMQC, TOCSY-HMQC, and HNHA experiments, the 3D $^{13}C$-separated NOESY and HCCH-TOCSY experiments, the CBCANNH experiment, and the 2D [F1-C/N, F2-C/N]-NOESY and [F2-C/N]-NOESY experiments were recorded on a Bruker AMX600 spectrometer. All the data were processed using the AZARA software package (W. Boucher, unpublished) and analyzed with the program ANSIG 3.3 (*24*) on Silicon Graphics Iris workstations. Both programs are available by anonymous ftp to ftp.bio.cam.ac.uk in the directory ~ftp/pub. The heteronuclear NOEs were derived from peak intensities according to the definition of Noggle and Schirmer (*25*). Sequential $^1H$ and $^{15}N$ chemical shift assignments in the protein backbone were made for the holo domain using 2D DQF-COSY (*26*) and 3D $^{15}N$-separated TOCSY-HMQC and NOESY-HMQC (*27*) experiments. The assignments were later confirmed for both the holo and apo domains by 3D CBCANNH experiments (*28*). Aliphatic side chain assignments were made using 3D $^{15}N$-separated

TOCSY-HMQC and $^{13}$C-separated HCCH-TOCSY (*29*) experiments by making reference to a high-resolution constant-time [$^{13}$C,$^{1}$H]-HSQC spectrum (*30*). The unlabeled biotin group was assigned using two isotope-filtered 2D experiments: [F1-C/N, F2-C/N]-NOESY and [F2-C/N]-NOESY (*31*).

*Structural Constraints and Structure Calculations*. Through-space nuclear Overhauser effect (NOE) connectivities were obtained from 2D NOESY (*32*), 3D $^{15}$N-separated NOESY-HMQC, and 3D $^{13}$C-separated NOESY (*33*, *34*) spectra. From these spectra, cross-peaks exhibiting strong, medium, and weak intensities were converted into distance restraints of 1.8−2.8, 1.8−3.5, and 1.8−5.0 Å, respectively. Vicinal coupling constants between amide and $^{1}$H$^{\alpha}$ spins ($^{3}J_{\alpha N}$) were determined by least-squares fitting to the intensities of cross-peaks from a set of 2D *J*-modulated [$^{15}$N,$^{1}$H]-COSY experiments (*35*). Estimates of the backbone angle $\phi$ were made by reference to a Karplus curve (*36*). For the apo domain, backbone $\phi$ angles were determined from a 3D $^{15}$N-separated HNHA experiment (*37*). Using a combination of HNHB (*38*), $^{15}$N-separated NOESY-HMQC, and TOCSY−HMQC spectra of the holo domain, the most populated $\chi_1$ rotamer and stereospecific assignments of $^{1}$H$^{\beta}$ resonances could be identified for 10 residues (*39*). Slowly exchanging amide protons were identified by recording a series of [$^{15}$N,$^{1}$H]-HSQC spectra (*40*, *41*) of lyophilized protein samples immediately after they had been redissolved in $^{2}H_2O$. Structures were calculated from the NMR data using the program X-PLOR (*42*), but with minor modifications to the files sa.inp and refine.inp from the X-PLOR 3.1 release (M. Nilges, personal communication). The computations were performed starting from random initial structures and using "sum" averaging with an $r^{-6}$ potential (*43*, *44*) for all atoms.

## RESULTS AND DISCUSSION

*Expression and $^{15}$N and $^{13}$C Labeling of the Holo and Apo Biotinyl Domains*. The biotinyl domain was expressed from a subgene encoding the 87 C-terminal amino acids, residues Met70−Glu156, of BCCP from *E. coli* ACC. The biotinylated lysine residue is at position 122. The protein was expressed and purified as described in Materials and Methods to produce uniformly $^{13}$C- and $^{15}$N-labeled, $^{15}$N-labeled, and unlabeled apo and holo biotinyl domains. In all cases, the biotinyl moiety was unlabeled (see Materials and Methods). Analysis of the purified protein samples by PAGE under denaturing and nondenaturing conditions (*7*) indicated that the samples were homogeneous. The purity and identity of the proteins were confirmed by electrospray mass spectrometry and N-terminal sequencing, carried out as described by Chapman-Smith et al. (*7*). The mass determined for the $^{15}$N holo biotinyl domain was 9662.78 ± 1.18 Da, within 0.6 Da of the mass expected for uniform $^{15}$N labeling (9663.4 Da). For the doubly labeled proteins, the masses determined were 9838.28 ± 0.73 and 10 064.77 ± 1.30 Da for the apo and holo forms, respectively, compared with masses of 9839.48 and 10 065.58 Da expected for uniform $^{13}$C and $^{15}$N labeling with 98% isotopic abundance. The preparations of apo or holo protein were each free of the other form of the domain (data not shown).

*NMR Assignment Strategy*. Sequential $^{1}$H and $^{15}$N chemical shift assignments in the protein backbone were made for the holo domain using 2D DQF-COSY and 3D $^{15}$N-separated TOCSY-HMQC and NOESY-HMQC experiments. The assignments were later confirmed for both the holo and apo domains by 3D CBCANNH experiments. Aliphatic side chain assignments were made using 3D $^{15}$N-separated TOCSY-HMQC and $^{13}$C-separated HCCH-TOCSY experiments by making reference to a high-resolution constant-time [$^{13}$C,$^{1}$H]-HSQC spectrum. The unlabeled biotin group was assigned using two isotope-filtered 2D experiments: [F1-C/N, F2-C/N]-NOESY and [F2-C/N]-NOESY. Residues 70−74 yielded very weak amide signals because of rapid exchange with the solvent; consequently, cross-peaks from these residues were left unassigned.

*Determination of Structural Constraints*. For the holo domain, 679 inter-residue NOEs were identified, including 23 NOEs to the biotin moiety. For the apo domain, 802 inter-residue connections were found. For the holo domain, vicinal coupling constants between amide and $^{1}$H$^{\alpha}$ spins ($^{3}J_{\alpha N}$) were determined by least-squares fitting to the intensities of cross-peaks from a set of 2D *J*-modulated [$^{15}$N,$^{1}$H]-COSY experiments, permitting estimates of the backbone angle $\phi$ for 30 residues. For the apo domain, 27 backbone $\phi$ angles were determined from a 3D $^{15}$N-separated HNHA experiment. Using a combination of HNHB, $^{15}$N-separated NOESY-HMQC, and TOCSY-HMQC spectra of the holo domain, the most populated $\chi_1$ rotamer and stereospecific assignments of $^{1}$H$^{\beta}$ resonances could be determined for 10 residues; in addition, $\chi_1$ rotamer assignments were made for eight valine, six isoleucine, and three threonine residues. For the holo domain, a total of 51 slowly exchanging amide protons were identified by recording a series of [$^{15}$N,$^{1}$H]-HSQC spectra on a lyophilized protein sample immediately after it had been redissolved in $^{2}H_2O$; 31 of these were used in hydrogen bond restraints in the final round of structure calculations. For the apo domain, in similar experiments 45 amide protons were found to exchange slowly, 30 of which were used as hydrogen bond restraints.

*Structure Calculations*. Preliminary structures for the holo and apo domains were computed from simulated annealing calculations using the program XPLOR 3.1 (*42*) based on 1390 and 1732 $^{1}$H−$^{1}$H distance restraints, respectively; these restraints could be determined unambiguously from unique chemical shift information alone. These sets of initial structures were used to assist in the selection of acceptor carbonyl oxygen atoms for hydrogen bonds with the slowly exchanging backbone amide protons.

For the holo domain, the final round of calculations used a constraint list comprising 1390 unambiguous distance restraints (of which 668 were intraresidue), 22 semiambiguous distance restraints (*44*), 30 $\phi$ and 27 $\chi_1$ dihedral angle restraints, and 31 hydrogen bonds. The selected ensemble is displayed as a backbone trace in Figure 1a and contains 23 structures (those with the lowest energies and no distance violations of >0.5 Å) out of the 40 that were calculated. For the apo domain, the final restraint list consisted of 1732 unambiguous distance restraints (of which 842 were intraresidue), 13 $\phi$ dihedral angle restraints, and 30 hydrogen bonds. Out of the 40 calculated structures, 20 converged structures were selected for the final ensemble (Figure 1b).

The structures of both forms of the biotinyl domain are well-defined, except for the first 10 amino acid residues at the N-terminus. Residues 70−79 are genuinely flexible in

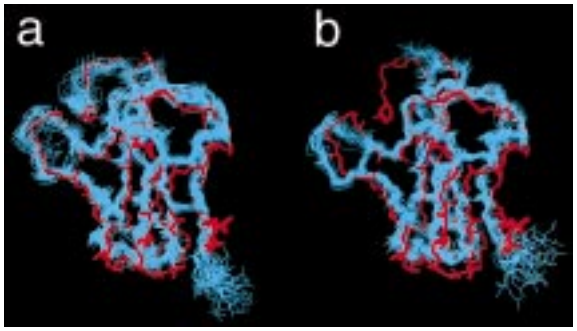


FIGURE 1: Structure of the biotinyl domain of *E. coli* BCCP. (a) Superposition of backbone traces from the final ensemble of 23 solution structures of the holo biotinyl domain in blue, with the crystal structure of the holo domain in red. (b) Superposition of backbone traces from the final ensemble of 20 solution structures of the apo domain in blue, with the crystal structure of the holo domain in red. The biotinyl-lysine residue is at position 122 (BCCP numbering). This figure was generated using the program MOLSCRIPT (*63*).

solution, as judged by studies of the steady state $\{^1H\}-^{15}N$ heteronuclear Overhauser effect ($\{^1H\}-^{15}N$ NOE) (*45*), which probes the sub-nanosecond dynamics of backbone amide sites (Figure 2a). The amino acid sequence up to residue 79 represents part of the flexible interdomain linker between the biotinyl and subunit-binding domains of BCCP, whereas the polypeptide chain between residues 80 and 156 is structured. Over residues 80−156, the root-mean-square deviation (rmsd) is 0.79 ± 0.19 Å for the backbone $C^\alpha$ atoms in the holo domain ensemble, while the rmsd for all heavy atoms is 1.23 ± 0.21 Å; over the restricted range between residues 80−95 and 100−156, the $C^\alpha$ rmsd is 0.64 ± 0.12 Å and the heavy atom rmsd is 1.13 ± 0.15 Å. For the apo domain ensemble, the $C^\alpha$ rmsd is 0.50 ± 0.07 Å between residues 80 and 156 and the heavy atom rmsd is 0.97 ± 0.09 Å. The structures have good covalent geometry, as judged by PROCHECK (*46*); for a list of relevant statistics, see Table 1.

*Comparison of Solution and Crystal Structures of the Holo Domain*. A polypeptide fragment comprising residues 77−156 released by proteolysis was used to determine the X-ray crystal structure of the C-terminal domain of holo-BCCP (*20*), in contrast to the longer 87-residue fragment encoded by a subgene studied here. The crystallographic *B*-factors for residues 77−80 are large (Figure 2b). Likewise, large negative values of the $\{^1H\}-^{15}N$ NOE (Figure 2a) show that the backbone amide sites of residues 70−79 are flexible on the sub-nanosecond time scale (*47*). Similarly, we do not expect the additional N-terminal residues in the protein that was used for the NMR experiments to contribute to any structural differences between the two systems.

The crystal and solution structures of the holo domain overlay closely, the rmsd of the backbone $C^\alpha$ atoms being 1.62 ± 0.16 Å over residues 80−156 and 1.47 ± 0.09 Å over the restricted range of residues 80−95 and 100−156. A residue-by-residue comparison of backbone $C^\alpha$ rmsds (Figure 2c) and crystallographic *B*-factors (Figure 2b) shows that the NMR ensemble is not as well defined in the surface-exposed thumb formed by residues 95−100. The same region also exhibits increased *B*-factors in the X-ray data. Both structures consist of two sets of four antiparallel $\beta$-strands in the form of a capped $\beta$-sandwich with a quasi-dyad axis

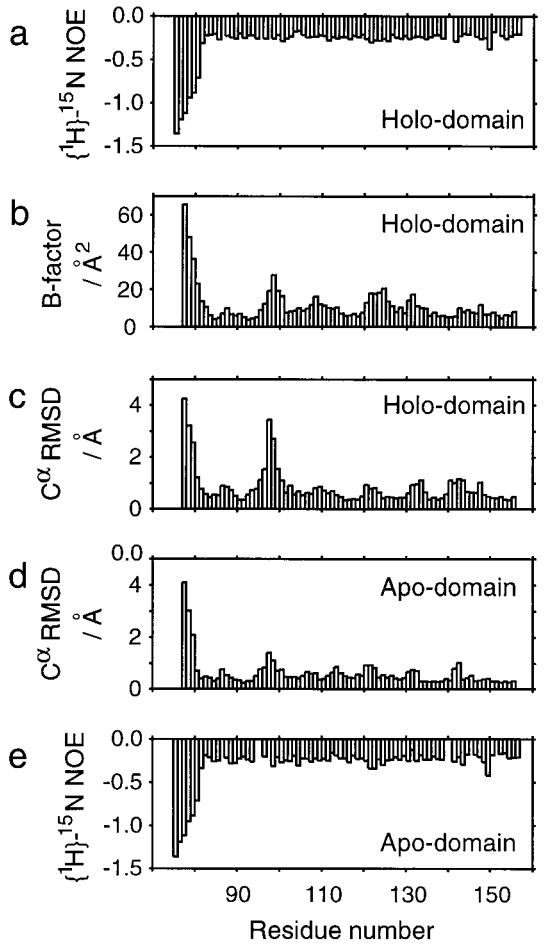


FIGURE 2: Structure parameters for the biotinyl domain of *E. coli* BCCP. (a) Plot of the heteronuclear $\{^1H\}-^{15}N$ NOE vs residue number for the holo domain. (b) Plot of the crystallographic *B*-factor for $C^\alpha$ atoms from the X-ray study of the holo domain (*20*). (c) Plot of the root-mean-square deviation of the backbone $C^\alpha$ atom positions from the average structure for the final ensemble of the holo domain. (d) Plot of the root-mean-square deviation of the backbone $C^\alpha$ atom positions from the average structure for the final ensemble of the apo domain. (e) Plot of the heteronuclear $\{^1H\}-^{15}N$ NOE vs residue number for the apo domain.

of symmetry and a hairpin protrusion between residues 93 and 102 (see Figure 3a). The first $\beta$-sheet is formed by strands $\beta$2, $\beta$4, $\beta$5, and $\beta$7, while the second consists of strands $\beta$1, $\beta$3, $\beta$6, and $\beta$8. The elements of secondary structure found in the X-ray study can also be identified in the present experiments from $^1H^\alpha$, $^{13}C^\alpha$, and $^{13}C^\beta$ chemical shifts (*48*), patterns of short- and intermediate-range inter-residue NOEs, $^3J_{\alpha N}$ couplings, and amide exchange rates (*49*), summarized in Figure 4a. Bulges are observed in strands $\beta$4, $\beta$6, and $\beta$8, giving rise to strong $H^N-H^N$ NOEs between residues 115 and 116, 136 and 137, and 152 and 153; this is consistent with values of the torsion angle $\psi$ of around −45° for residues 115, 136, and 152 in the crystal structure (*50*).

When the $[^{15}N,^1H]$-HSQC spectrum of the holo domain was recorded after replacing the $^1H_2O$ solvent with $^2H_2O$, 53 peaks remained. Six of these were weak enough to disappear after 30 min, leaving 47 peaks from residues that were substantially protected from solvent exchange. Out of these 47 peaks, 26 could be matched to the same hydrogen bond donor−acceptor pairs identified in the crystal structure, but one hydrogen bond donor assigned from the crystal

Table 1: Structural Statistics for the Final Ensembles of Refined Structures of the Holo and Apo Forms of the Biotinyl Domain of *E. coli* BCCP

| | Root-Mean-Square Deviations from Restraints and Idealized Geometry | | | |
|---|---|---|---|---|
| | holo | | apo | |
| | $\langle SA \rangle^a$ | $(SA)_{clo}{}^b$ | $\langle SA \rangle^a$ | $(SA)_{clo}{}^b$ |
| NOE distances (Å) | 0.013 ± 0.005 | 0.008 | 0.018 ± 0.003 | 0.015 |
| dihedral angles (deg) | 0.92 ± 0.61 | 1.1 | 0.65 ± 0.72 | 1.4 |
| bonds (Å) | 0.0011 ± 0.0001 | 0.0010 | 0.0014 ± 0.0001 | 0.0013 |
| angles (deg) | 0.37 ± 0.15 | 0.37 | 0.39 ± 0.01 | 0.38 |
| impropers (deg) | 0.09 ± 0.01 | 0.01 | 0.12 ± 0.01 | 0.11 |
| size of ensemble | 23/40 | | 20/40 | |
| final energy $E_{L-J}$ (kJ/mol) | −507.1 ± 98.3 | −421.7 | −241.0 ± 88.7 | −273.6 |
| | Assessment of Backbone Quality According to the Ramachandran Plot | | | |
| | holo | | apo | |
| most favored region | 51.2%[c] | 53.6%[b] | 40.5%[c] | 48.5%[b] |
| additionally allowed region | 41.2%[c] | 40.0%[b] | 53.4%[c] | 45.6%[b] |

[a] Represents the average root-mean-square deviation for the ensemble. [b] Represents the values for the final structure that is closest to the mean. [c] Represents the values for all the structures in the ensemble.

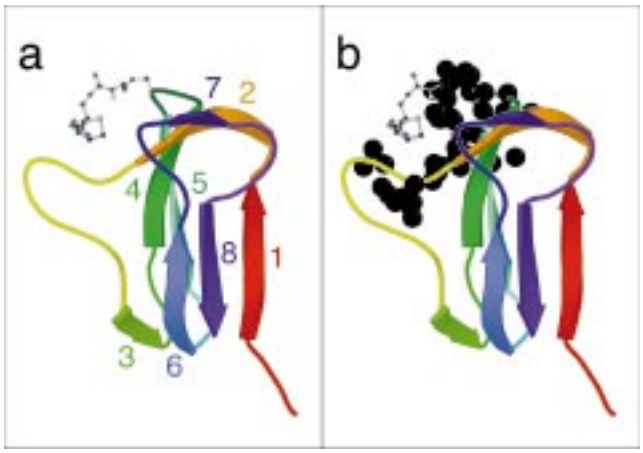


FIGURE 3: Schematic representations of the structure of the biotinyl domain of *E. coli* BCCP. (a) Representation of the solution structure of the holo domain, in the same orientation as the ensemble shown in Figure 1a, showing the biotinyl prosthetic group (attached to K122) at the top left, the protruding thumb in yellow, and the $\beta$-strands numbered and coded from red at the N-terminus to indigo at the C-terminus. (b) Representation of the solution structure of the holo domain, with black spheres marking the locations of atoms that display significant changes in chemical shift between the apo and holo forms. The color coding is like that in panel a. This figure was generated using the program MOLSCRIPT (*63*).

structure (H81 $H^N$) appears to exchange too rapidly to be detected in the first exchange experiment. Two donors from the X-ray structure (T90 $H^N$ and L139 $H^N$) seem to match up to different acceptor partners in the NMR ensemble (V118O and P151O instead of E119O and L152O, respectively). New hydrogen bond acceptors could be identified for a further five $H^N$ donors, leaving 14 amides for which suitable acceptors could not be identified; these sites are protected from exchange because they are buried by the tertiary fold of the protein.

Athappilly and Hendrickson (*20*) noted that the biotinylated lysine is located at a type I′ hairpin turn between strands $\beta$4 and $\beta$5, which is stabilized by three hydrogen bonds: A120 $H^N \cdots$O M123, K122 $H^N \cdots O^{\epsilon 2}$ E119, and M123 $H^N \cdots$O A120. The observed pattern of NOEs supports the classification of the $\beta$-turn, as retarded $H_N$ exchange rates were found for A120 $H^N$ and M123 $H^N$, indicating that these residues are indeed hydrogen bond donors. The signal ascribed to the amide proton of residue 122 disappeared within the 5 min dead time of the solvent exchange experiment, suggesting that the K122 $H^N \cdots O^{\epsilon 2}$ E119 hydrogen bond may be an artifact of the crystal environment. In agreement with the X-ray structure, both strands $\beta$3 and $\beta$7 are bracketed by two type II turns and, as found in a previous NMR study of an apo domain (*21*), there is a $\beta$-turn between residues 96 and 99 which is difficult to classify because of the exposure to the solvent. The buried hydrophobic core of the domain is formed by the side chains of residues V83, S85, F91, I103, V109, L115, C116, I117, V118, A129, V135, V146, L152, V153, V154, and I155, which all have a fractional surface area (*51*) of less than 0.30, in accord with the crystal structure.

As in the X-ray structure (*20*), the biotin prosthetic group is well-defined in the NMR ensemble (Figure 1a); the heavy atoms have a rmsd of 0.94 ± 0.45 Å. The biotinyl-lysine side chain (K122) is not freely moving, being restrained by the interatomic connections summarized in Table 2, which include contacts with five residues in the protruding hairpin. In the NMR ensemble, the biotin moiety possesses a fractional surface area of 0.47, lying on the surface of the domain and protecting the backbone NH protons of residues T94 and S96 from exchange with the solvent. The proton chemical shifts of the biotinyl group in the holo domain differ substantially from those measured in both free biotin and the biotinyl moiety of the 1.3S subunit of transcarboxylase (*22*), the largest changes being located on the face that makes contact with the domain. In the crystal structure of the ACC biotinyl domain, the side chain and main chain oxygen atoms of T94 were shown to form hydrogen bonds with the ureido $O^{2'}$ carbonyl and $N^{1'}$ amide atoms of biocytin, respectively (*20*). However, in our deuterium exchange experiments, signals from both the $H^{N1'}$ and $H^{N3'}$ amide protons of the biotinyl moiety disappeared within 5 min of replacing the $H_2O$ solvent with $D_2O$. The exchange rate of $H^{N1'}$ is thus not retarded several orders of magnitude, as might be expected in the case of protection by a strong hydrogen bond between $N^{1'}$ and T94 O. Saturation transfer experiments (data not shown) indicate that the exchange rates of $H^{N1'}$ and $H^{N3'}$ are in fact similar to those found in free biotin and the holo 1.3S domain of transcarboxylase (22), suggesting that a strong hydrogen bond between the $N^{1'}$ atom and T94 O does

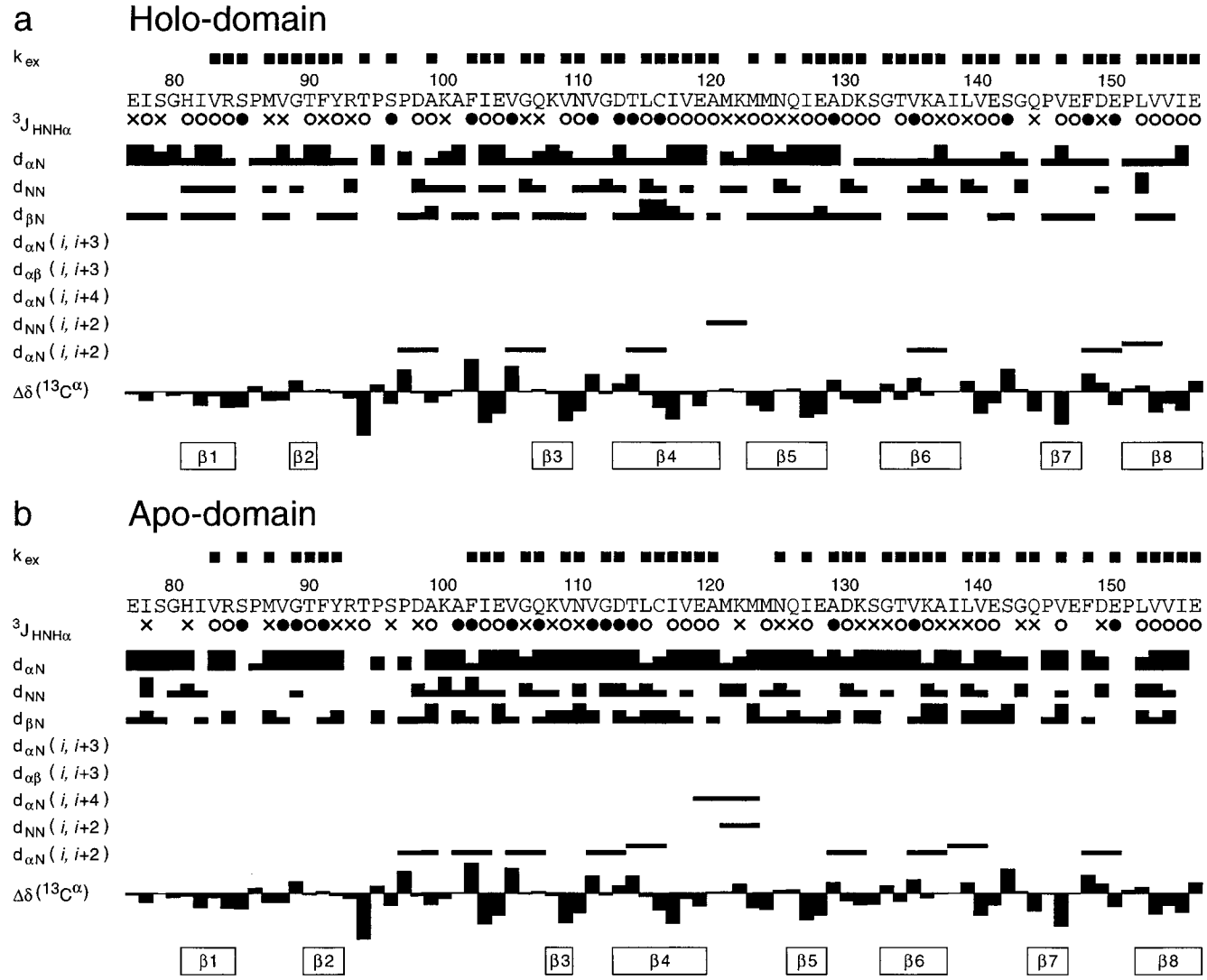


FIGURE 4: Summary of the data used in the secondary structure determination of the biotinyl domain of *E. coli* BCCP. (a) Amino acid sequence and summary of the amide proton exchange data, $^3J_{\alpha N}$ coupling constants, sequential NOEs, and $C^\alpha$ secondary shifts used in determining the secondary structure of the holo domain. For $k_{ex}$, filled boxes indicate amide sites not fully exchanged after 5 min. (●) $^3J_{\alpha N} < 5$ Hz, (×) 5 Hz $< {}^3J_{\alpha N} < 8$ Hz, and (○) $^3J_{\alpha N} > 8$ Hz. For NOEs, the height of the bar indicates the strength of the NOE (strong, medium, or weak). The biotinyl-lysine is at position 122. (b) Summary of secondary structure data for the apo domain.

Table 2: Weak NOEs from the Biotin Moiety and K122 Observed in NOESY Experiments for the Holo but Not for the Apo Form of the Biotinyl Domain of *E. coli* BCCP[a]

| | |
|---|---|
| $H^{N1'}$−Y92 $H^{\beta2/\beta3}$ | $H^4$−I117 $H^{\gamma2}$ |
| $H^{N1'}$−Y92 $H^{\delta1/\delta2}$ | $H^{5a/5b}$−Y92 $H^{\delta1/\delta2}$ |
| $H^{N1'}$−T94 $H^N$ | $H^{5a}$−Y92 $H^{\epsilon1/\epsilon2}$ |
| $H^{N1'}$−S96 $H^N$ | $H^{5b}$−Y92 $H^{\epsilon1/\epsilon2}$ |
| $H^{N1'}$−P97 $H^{\gamma2}$ | $H^{5a/5b}$−I117 $H^{\gamma2}$ |
| $H^{N1'}$−P97 $H^{\gamma3}$ | $H^{5a}$−I117 $H^{\delta1}$ |
| $H^{N1'}$−S96 $H^\alpha$ | $H^{5b}$−I117 $H^{\delta1}$ |
| $H^{N3'}$−Y92 $H^{\delta1/\delta2}$ | $H^{7a/7b}$−K122 $H^\zeta$ |
| $H^{N3'}$−Y92 $H^{\epsilon1/\epsilon2}$ | $H^{8a/8b}$−K122 $H^\zeta$ |
| $H^2$−Y92 $H^{\delta1/\delta2}$ | |
| $H^2$−Y92 $H^{\epsilon1/\epsilon2}$ | K122 $H^\alpha$−M124 $H^\epsilon$ |
| $H^3$−Y92 $H^{\delta1/\delta2}$ | K122 $H^{\beta2/\beta3}$−M124 $H^N$ |
| $H^3$−Y92 $H^{\epsilon1/\epsilon2}$ | K122 $H^{\delta2/\delta3}$−M124 $H^\epsilon$ |
| $H^3$−P95 $H^\alpha$ | K122 $H^N$−A120 $H^N$ |
| $H^4$−Y92 $H^{\delta1/\delta2}$ | K122 $H^\zeta$−E119 $H^{\beta2/\beta3}$ |
| $H^4$−Y92 $H^{\epsilon1/\epsilon2}$ | K122 $H^\zeta$−E119 $H^{\gamma2/\gamma3}$ |

[a] The nomenclature for the biotin moiety is taken from ref *22*.

not exist in solution. In addition, the T94 $O^\gamma$ is more than 5 Å from the ureido $O^{2'}$ atom in the solution structure, also making this hydrogen bond unlikely.

In the NMR ensemble, it appears that the hairpin between strands $\beta4$ and $\beta5$ adopts an orientation different from that found in the X-ray structure. There is a superhelical twist defined by NOEs observed between the side chain $H^{\delta2}$ protons of N125 and the backbone amide proton and methyl group of A120; these atoms are separated by more than 7 Å in the crystal structure. Corresponding connections were also encountered in the previous NMR study of an apo domain by Yao et al. (*21*), as well as in our apo domain structure, discussed below. In contrast with the conclusion of Yao et al. (*21*), we find that the ureido ring of the biotinyl moiety is still able to interact with the thumb formed by the residues R93−F102 when the $\beta4-\beta5$ hairpin is twisted, as illustrated by the contacts listed in Table 2.

*Comparison of Solution Structures of Holo and Apo Domains*. The solution structures of holo and apo biotinyl domains determined in this work are very similar (Figure 1a,b). An overlay of the structures that are closest to the mean from each ensemble gives a backbone $C^\alpha$ rmsd of 1.29 Å over residues 80−156. There is clearly no major change in conformation of the domain that accompanies post-

translational modification, as was found also for the lipoyl domains of 2-oxo acid dehydrogenase complexes (*13*). As shown in Figure 2d, the apo domain ensemble has less variation in the exposed hairpin between R93 and F102. The apo domain structure differs a little more from the crystal structure (*20*) of the holo domain, possessing backbone $C^{\alpha}$ rmsds of 1.89 ± 0.08 Å between residues 80 and 156 and 1.63 ± 0.07 Å over the sections comprising residues 80−95 and 100−156. This may be compared with the work of Yao et al. (*21*), whose superposition of the backbone heavy atoms of their solution structure for the apo domain with the X-ray structure of the holo domain afforded an average rmsd of 1.21 Å between residues 80 and 156. The $\beta$-strands identified in our ensemble are shown in Figure 4b; bulges similar to those found in the holo domain solution structure (see above) are found in strands $\beta$4, $\beta$6, and $\beta$8 between residues 115 and 116, 136 and 137, and 152 and 153, respectively. In agreement with Yao et al. (*21*), our apo domain structure shows the same superhelical twist of the $\beta$4−$\beta$5 hairpin; however, we were able to detect some through-space connections predicted from the crystal structure of the holo domain that were not present in their NOESY spectra, for example, the weak NOE between A120 $H^N$ and M121 $H^N$.

Of the 45 protected backbone sites identified in our deuterium exchange experiment for the apo domain, 29 could be matched to the same hydrogen bond donor−acceptor pairs identified in the crystal structure of the holo domain, including T90 $H^N$ and L139 $H^N$. In contrast with their behavior in the holo domain, the amide protons of residues T94, S96, and A99 exchanged rapidly in the apo domain; these sites are no longer protected from the solvent once the prosthetic group has been removed.

Chemical shift differences between the holo and apo forms of the biotinyl domain are summarized for $^1H$, $^{15}N$, and $^{13}C$ nuclei in Figure 5. In all, 37 sites were found to have chemical shift changes that are more than two standard deviations from the mean. All of these correspond to regions of the protein that are in close proximity to the biotinyl group (Figure 3b), with most lying in two clusters: residues close to K122, to which the prosthetic group is covalently attached; and others in the protruding hairpin between residues Y92 and F102. Small chemical shift changes were also evident in the nearby turn between strands $\beta$6 and $\beta$7. Such localized changes in chemical shift confirm that significant changes in the electronic environment are confined to nuclei that are close to the biotinyl group and that there is no substantial change in the structure of the protein domain on post-translational modification.

The steady state $\{^1H\}-^{15}N$ NOE values for the holo domain and apo domain, presented in panels a and e of Figure 2, respectively, show large negative values from the N-terminus up to residue 80. Beyond this, the mean values of the NOE are −0.24 ± 0.03 and −0.23 ± 0.05 for the holo and apo domain, respectively, both of which are close to the expected theoretical value of −0.25 for backbone amide sites with no significant contribution to relaxation from sub-nanosecond internal motions (*47*). This last result contradicts the work of Yao et al. (*21*), who found evidence of rapid internal motion for several residues in the protruding thumb (S96−A99) and the biotin-binding turn (K122−A129) in experiments carried out at pH 7.5 and 25 °C. At high pH,

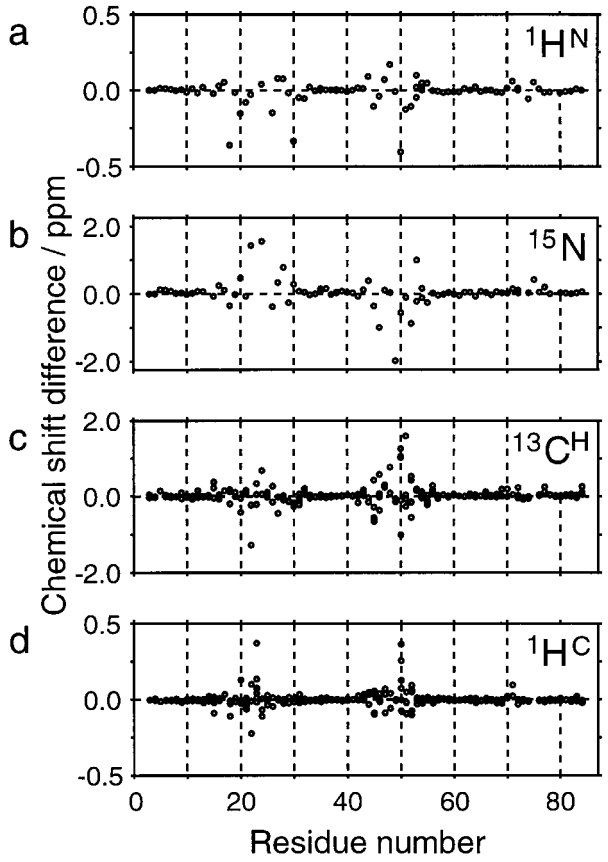


FIGURE 5: Chemical shift differences between the holo and apo forms of the biotinyl domain of *E. coli* BCCP plotted vs residue number: (a) backbone and side chain amide proton sites, (b) backbone and side chain amide nitrogen sites, (c) $^{13}C^{\alpha}$ and side chain carbon sites, and (d) $^1H^{\alpha}$ and residual side chain proton sites.

when exchange of amide protons with the solvent can be very rapid and solvent magnetization transfer can have large effects, modifications (*45*) are necessary to ensure the accuracy of all the experiments needed to measure $^{15}N$ relaxation parameters (R. W. Broadhurst and D. Nietlispach, unpublished work). We found several backbone amide sites in the two regions considered to be highly susceptible to solvent saturation transfer, especially those of residues T94, S96, and M121.

Yao et al. (*21*) also reported that multiple interactions between the ureido ring of the biotinyl group and the residues in the protuding thumb confer a strained conformation on the biotinyl-lysine turn, which does not exist in the apo domain. We see no clear evidence of this.

*Relationship to Biological Activity*. The solution structure for the biotinyl domain of the BCCP of *E. coli* acetyl CoA carboxylase described above is in excellent agreement with the crystal structure of the same protein determined elsewhere (*20*) in almost all respects. In particular, the biotinyl-lysine side chain is not freely moving on the surface of the protein, but is localized by interactions with the protein, chiefly with the projecting thumb region formed by residues 95−100. It is now clear that this cannot be an artifact of the crystallization conditions but is a property of the native protein in solution. It stands in marked contrast with the biotinyl-lysine residue in the 1.3S subunit of transcarboxylase from *P. shermanii*, for which no evidence of strong protein−biotin interactions was found with NMR spectroscopy (*22*). Amino

acid sequence alignments [see, for example, Samols et al. (*9*)] indicate that the thumb region is an insertion in the *E. coli* BCCP domain and other bacterial ACCs, and is lacking in almost all other biotinyl domains, including that from the *P. shermanii* transcarboxylase. Thus, it may be that the localization of the biotinyl-lysine residue in the BCCP protein is an unusual event, with a particular requirement in the ACC reaction.

One interesting difference between the crystal (*20*) and solution structures for the holo form of the ACC biotinyl domain is the lack of a strong hydrogen bond between the main chain oxygen atom of T94 and the ureido $H^{N1'}$ atom of the biotinyl group, as judged by deuterium exchange experiments (see above). This amide nitrogen is the site of carboxylation of the biotin by the BC component of ACC, and our results indicate that no strong hydrogen bond needs to be broken to achieve this, although it would appear that the biotinyl group must be displaced from the surface of the domain for carboxylation to occur.

An intriguing question is how the particular lysine residue in the biotinyl domain is selected for post-translational modification. This reaction is catalyzed by a biotinyl protein ligase, the 3D structure of which in *E. coli* has been determined by X-ray crystallography (*52*). It has been demonstrated that the highly conserved MKM sequence housing the target lysine residue is not necessary but that correct positioning of the lysine in the protruding $\beta$-turn is essential (*53*). Likewise, the biotinyl protein ligase must be able to distinguish the biotinyl domain from the structurally homologous lipoyl domains of 2-oxo acid dehydrogenase complexes to avoid aberrant modification. The determination of the 3D structure of the apo form of the domain (*21*; above work) should aid in understanding the protein−protein interactions with the ligase that make this possible. However, the lack of any major difference between the structures of the holo and apo forms of the biotinyl domain of *E. coli* BCCP described above may not be wholly reflected in their behavior in solution. Thus, the packing of side chains is more favorable in the holo domain (Table 1), the lower energy indicating a difference in the inherent stabilities of the two forms of the protein. Similarly, it has been found that C116 in the apo domain is capable of reaction with thiol reagents, unlike the same residue in the biotinylated domain, and that the apo protein is considerably more susceptible to several proteinases than the holo protein (*54*). These observations may be due to differences in the dynamics of the structures of the apo and holo domains, which are picked up by the irreversible nature of the chemical modification and limited proteolysis reactions.

The localization of the biotinyl-lysine residue in the biotinyl domain of *E. coli* BCCP contrasts with the freedom to move enjoyed by the lipoyllysine residue similarly located in the homologous lipoyl domains (*12*, *13*, and references therein). The only example of a localized lipoyllysine residue to date is the H-protein of the pea leaf glycine cleavage system (*55*). In this instance, the lipoyllysine residue is also localized when it becomes reductively aminomethylated as part of the enzymic reaction (*56*), but it is found then to occupy a different position, tucked in a surface cleft that protects the labile intermediate from breakdown in aqueous solution before it can reach the next enzyme active site. This makes it an elegant example of the "hot potato hypothesis" advanced as a possible advantage to be conferred by a multienzyme system (*57*). In the case of the *P. shermanii* transcarboxylase, it has been proposed from an NMR study that the distance between the two subsites of substrate carboxylation may be as short as 0.7 nm (*58*), a figure consistent with an X-ray study of biotin derivatives which showed that a simple intramolecular rotation about two single bonds of carboxybiotin could alter the position of the $N^{1'}$ carboxylate carbon by 0.69 nm (*59*). However, it would appear that not all the evidence supports this view (*60*). With the biotinyl domain of *E. coli* BCCP, there is no obvious reason the biotinyl-lysine residue should be constrained before its carboxylation by the BC subunit of ACC and the carboxylated biotin is stable (*5*, *61*). These considerations make it important now to determine the structure of the carboxylated form of the holo domain.

In the 2-oxo acid dehydrogenase complexes, attachment of the lipoyl group to the lipoyl domain is essential for it to act as an effective substrate for reductive acylation by the E1 (2-oxo acid decarboxylase) component ($k_{cat}/K_m$ raised by a factor of $10^4$); moreover, the domain confers specificity for reductive acylation by only the partner E1 (*62*). Similar considerations apply to the biotinyl group in most biotin-dependent carboxylases; i.e., free biotin is a poor substrate for carboxylation (*5*). One of the few exceptions is *E. coli* ACC, which may point to the unexpected localization of the biotinyl-lysine swinging arm on its biotinyl domain. The structures of the holo and apo forms of the biotinyl domain will clearly serve as an important starting point for understanding these and the other fundamental questions about the mode of action of biotin-dependent carboxylases and the mechanistic parts played by their swinging arms.

## ACKNOWLEDGMENT

We thank Dr. A. R. C. Raine for assistance with the structure calculations and Mr. C. Fuller and Dr. D. Nietlispach for skilled technical assistance.

## SUPPORTING INFORMATION AVAILABLE

Two tables summarizing the chemical shifts of the apo and holo biotinyl domains. This material is available free of charge via the Internet at http://pubs.acs.org.

## REFERENCES

1. Guchhait, R. B., Polakis, S. E., Dimroth, P., Stoll, E., Moss, J., and Lane, M. D. (1974) *J. Biol. Chem. 249*, 6633−6645.
2. Fall, R. R., and Vagelos, P. R. (1972) *J. Biol. Chem. 247*, 8005−8015.
3. Li, S.-J., and Cronan, J. E., Jr. (1992) *J. Biol. Chem. 267*, 855−863.
4. Li, S.-J., and Cronan, J. E., Jr. (1992) *J. Biol. Chem. 267*, 16841−16847.
5. Knowles, J. R. (1989) *Annu. Rev. Biochem. 58*, 195−221.
6. Reed, K. E., and Cronan, J. E., Jr. (1991) *J. Biol. Chem. 266*, 11425−11428.
7. Chapman-Smith, A., Turner, D. L., Cronan, J. E., Morris, T. W., and Wallace, J. C. (1994) *Biochem. J. 302*, 881−887.
8. Nenortas, E., and Beckett, D. (1996) *J. Biol. Chem. 271*, 7559−7567.
9. Samols, D., Thornton, C. G., Murtif, V. L., Kumar, G. K., Haase, F. C., and Wood, H. G. (1988) *J. Biol. Chem. 263*, 6461−6464.
10. Reed, L. J., and Hackert, M. L. (1990) *J. Biol. Chem. 265*, 8971−8974.

11. Perham, R. N. (1991) *Biochemistry 30*, 8501−8512.
12. Berg, A., and de Kok, A. (1997) *Biol. Chem. 378*, 617−634.
13. Dardel, F., Davis, A. L., Laue, E. D., and Perham, R. N. (1993) *J. Mol. Biol. 229*, 1037−1048.
14. Ricaud, P. M., Howard, M. J., Roberts, E. L., Broadhurst, R. W., and Perham, R. N. (1996) *J. Mol. Biol. 264*, 179−190.
15. Berg, A., Vervoort, J., and de Kok, A. (1996) *J. Mol. Biol. 261*, 432−442.
16. Berg, A., Vervoort, J., and de Kok, A. (1997) *Eur. J. Biochem. 244*, 352−360.
17. Howard, M. J., Fuller, C., Broadhurst, R. W., Perham, R. N., Tang, J.-G., Quinn, J., Diamond, A. G., and Yeaman, S. J. (1998) *Gastroenterology 115*, 139−146.
18. Lim, F., Morris, C. P., Occhiodoro, F., and Wallace, J. C. (1988) *J. Biol. Chem. 263*, 11493−11497.
19. Brocklehurst, S. M., and Perham, R. N. (1993) *Protein Sci. 2*, 626−639.
20. Athappilly, F. K., and Hendrickson, W. A. (1995) *Structure 3*, 1407−1419.
21. Yao, X., Wei, D., Sodern, C., Summers, M. F., and Beckett, D. (1997) *Biochemistry 36*, 15089−15100.
22. Reddy, D. V., Shenoy, B. C., Carey, P. R., and Sönnichsen, F. D. (1997) *Biochemistry 36*, 14676−14682.
23. Neidhardt, F. C., Bloch, P. L., and Smith, D. F. (1974) *J. Bacteriol. 119*, 736−747.
24. Kraulis, P. J., Domaille, P. J., Campbell-Burke, S. L., Van Aken, T., and Laue, E. D. (1994) *Biochemistry 33*, 3515−3531.
25. Noggle, J. H., and Schirmer, R. E. (1971) *The Nuclear Overhauser Effect*, Academic Press, New York.
26. Rance, M., Sørensen, O. W., Bodenhausen, G., Wagner, G., Ernst, R. R., and Wüthrich, K. (1983) *Biochem. Biophys. Res. Commun. 117*, 479−485.
27. Marion, D., Driscoll, P. C., Kay, L. E., Wingfield, P. T., Bax, A., Gronenborn, A. M., and Clore, G. M. (1989) *Biochemistry 28*, 6150−6156.
28. Grzesiek, S., and Bax, A. (1992) *J. Magn. Reson. 99*, 201−207.
29. Bax, A., Clore, G. M., and Gronenborn, A. M. (1990) *J. Magn. Reson. 88*, 425−431.
30. Ogura, K., Terasawa, H., and Inagaki, F. (1996) *J. Magn. Reson., Ser. B 112*, 63−68.
31. Ikura, M., and Bax, A. (1992) *J. Am. Chem. Soc. 114*, 2433−2440.
32. Kumar, A., Ernst, R. R., and Wüthrich, K. (1980) *Biochem. Biophys. Res. Commun. 95*, 1−6.
33. Ikura, M., Kay, L. E., and Bax, A. (1990) *Biochemistry 29*, 4659−4667.
34. Zuiderweg, E. R. P., McIntosh, L. P., Dahlquist, F. W., and Fesik, S. W. (1990) *J. Magn. Reson. 86*, 210−216.
35. Billeter, M., Neri, D., Otting, G., Qian, Y. Q., and Wüthrich, K. (1992) *J. Biomol. NMR 3*, 349−354.
36. Pardi, A., Billeter, M., and Wüthrich, K. (1984) *J. Mol. Biol. 180*, 741−751.
37. Kubinowa, H., Grzesiek, S., Delaglio, F., and Bax, A. (1994) *J. Biomol. NMR 4*, 871−878.
38. Archer, S. J., Ikura, M., Torchia, D. A., and Bax, A. (1991) *J. Magn. Reson. 95*, 636−641.
39. Powers, R., Garrett, D. S., March, C. J., Frieden, E. A., Gronenborn, A. M., and Clore, G. M. (1993) *Biochemistry 32*, 6744−6762.
40. Bax, A., Ikura, M., Kay, L. E., Torchia, D. A., and Tschudin, R. (1990) *J. Magn. Reson. 86*, 304−318.
41. Norwood, T. J., Boyd, J., Heritage, J. E., Soffe, N., and Campbell, I. D. (1990) *J. Magn. Reson. 87*, 488−501.
42. Brünger, A. (1992) *X-PLOR, Version 3.1, A System for X-ray Crystallography and NMR*, Yale University Press, New Haven, CT.
43. Nilges, M., Clore, G. M., and Gronenborn, A. M. (1988) *FEBS Lett. 239*, 129−136.
44. Nilges, M. (1995) *J. Mol. Biol. 245*, 645−660.
45. Sørensen, M. D., Kristensen, S. N., and Led, J. J. (1995) *J. Magn. Reson., Ser. B 107*, 83−87.
46. Laskowski, R. A., Macarthur, M. W., Moss, D. S., and Thornton, J. M. (1993) *J. Appl. Crystallogr. 26*, 283−291.
47. Kay, L. E., Torchia, D. A., and Bax, A. (1989) *Biochemistry 28*, 8972−8979.
48. Wishart, D. S., and Sykes, B. D. (1994) *Methods Enzymol. 239*, 363−392.
49. Wüthrich, K. (1986) *NMR of Proteins and Nucleic Acids*, Wiley, New York.
50. Richardson, J. S. (1981) *Adv. Protein Chem. 34*, 167−339.
51. Hubbard, S. J., and Thornton, J. M. (1993) *NACCESS*, Computer Program, Department of Biochemistry and Molecular Biology, University College London, London, U.K.
52. Wilson, K. P., Shewchuk, L. M., Brennan, R. G., Otsuka, A. J., and Matthews, B. W. (1992) *Proc. Natl. Acad. Sci. U.S.A. 89*, 9257−9261.
53. Reche, P., Li, Y.-L., Fuller, C., Eichhorn, K., and Perham, R. N. (1998) *Biochem. J. 329*, 589−596.
54. Chapman-Smith, A., Forbes, B. E., Wallace, J. C., and Cronan, J. E. (1997) *J. Biol. Chem. 272*, 26017−26022.
55. Pares, S., Cohen-Addad, C., Sieker, L., Neuberger, M., and Douce, R. (1994) *Proc. Natl. Acad. Sci. U.S.A. 91*, 4851−4853.
56. Cohen-Addad, C., Pares, S., Sieker, L., Neuberger, M., and Douce, R. (1995) *Nat. Struct. Biol. 2*, 63−68.
57. Perham, R. N. (1975) *Philos. Trans. R. Soc. London, Ser. B 272*, 123−136.
58. Fung, C. H., Gupta, R. K., and Mildvan, A. S. (1976) *Biochemistry 15*, 85−92.
59. DeTitta, G. T., Parthasarathy, R., Blessing, R. H., and Stallings, W. (1980) *Proc. Natl. Acad. Sci. U.S.A. 77*, 333−337.
60. Wood, H. G., and Zwolinski, G. K. (1976) *CRC Crit. Rev. Biochem. 5*, 47−122.
61. Guchhait, R. B., Polakis, S. E., Hollis, D., Fenselau, C., and Lane, M. D. (1974) *J. Biol. Chem. 249*, 6646−6656.
62. Graham, L. D., Packman, L. C., and Perham, R. N. (1989) *Biochemistry 28*, 1574−1581.
63. Kraulis, P. J. (1991) *J. Appl. Crystallogr. 24*, 946−950.


BI982466O